

Centrifuge experiment and numerical analysis of an air-backed plate subjected to underwater shock loading

Zhijie HUANG^{a,b,c,d}, Xiaodan REN^{d*}, Zuyu CHEN^{a,b,c}, Daosheng LING^{a,b}

^a MOE Key Laboratory of Soft Soils and Geoenvironmental Engineering, Zhejiang University, Hangzhou 310058, China

^b Institute of Geotechnical Engineering, Zhejiang University, Hangzhou 310058, China

^c China Institute of Water Resources and Hydropower Research, Beijing 100048, China

^d School of Civil Engineering, Tongji University, Shanghai 200092, China

*Corresponding author: E-mail: rxdjtj@tongji.edu.cn

© Higher Education Press and Springer-Verlag GmbH Germany, part of Springer Nature 2019

ABSTRACT In this study, systematic centrifuge experiments and numerical studies are conducted to investigate the effect of shock loads due to an underwater explosion on the dynamic responses of an air-backed steel plate. Numerical simulations with three different models of pressure time history generated by underwater explosion were carried out. The first model of pressure time history was measured in test. The second model to predict the time history of shock wave pressure from an underwater explosion was created by Cole in 1948. Coefficients of Cole's formulas are determined experimentally. The third model was developed by Zamyshlyayev and Yakovlev in 1973. All of them are implemented into the numerical model to calculate the shock responses of the plate. Simulated peak strains obtained from the three models are compared with the experimental results, yielding average relative differences of 21.39%, 45.73%, and 13.92%, respectively. The Russell error technique is used to quantitatively analyze the correlation between the numerical and experimental results. Quantitative analysis shows that the simulated strains for most measurement points on the steel plate are acceptable. By changing the scaled distances, different shock impulses were obtained and exerted on the steel plate. Systematic numerical studies are performed to investigate the effect of the accumulated shock impulse on the peak strains. The numerical and experimental results suggest that the peak strains are strongly dependent on the accumulated shock impulse.

KEYWORDS underwater explosion, centrifuge experiment, shock load, dynamic response, accumulated shock impulse

1 Introduction

Navy ships and hydraulic structures (dams, decks, piers, etc.) tend to be targeted in wars or terrorist attacks. Therefore, to predict the shock response of these structures to underwater explosions (UNDEXs) is of particular importance for designers. In 1942, Kirkwood and Bethe [1] developed the theory to predict the pressure time history based on shock wave propagation theory. A seminal work (Underwater Explosions, Princeton Press) was written by R. H. Cole in 1948 on the UNDEX and the shock response of structures to UNDEX [2]. Keil [3] and

Reid [4] both conducted thorough government-sponsored studies on underwater explosives and damage to ships.

Generally, it is very difficult to develop an analytical solution for complicated UNDEX problems because the dynamic response of structures subjected to UNDEX depends not only on the detonation of explosives and shock wave propagation, but also on complex fluid-structure coupling interactions (FSI), such as the dynamic response of ships subjected to non-contact UNDEX [5]. Knowing the effects and causes of damage done is not just a matter of scientific interest but can help in the design of battle ships most likely to incur this type of damage. Numerical simulations have become the most common approach to UNDEX problem studies. Rabczuk et al. [6] developed the immersed particle method for treating fluid-structure interactions of fracturing structures. They also

presented a unified software framework for probabilistic sensitivity analysis for time-consuming models to quantify the effect of uncertain input parameters on uncertain model outputs [7]. Over the past decades, the commercial packages LS-DYNA and ABAQUS have been widely applied to the simulation of structural responses [8–11]. Shin [12] simulated the shock response of a ship using LS-DYNA and the results agreed well with test data. The effects of UNDEX on structures, the dynamic responses, and the damage of structures have been studied by numbers of researchers [13–18]. Some new meshfree particle methods [19–21] were proposed for structural fracture, which could be used to model discrete cracks for structures subjected to blast loading. Moreover, some new materials and techniques, such as polymeric nanoparticle composites [22] and flexoelectric nanostructures [23], can be used in the field of structural anti-explosion and structural health monitoring in the future.

Although numerical simulation could help predict the consequence of the explosions, numerical results would be more useful if they could be calibrated and validated by physical models [24]. As we know, full-scale tests of prototypes under UNDEX are costly, hazardous, and time-consuming. Therefore, small-scale testing of UNDEX is usually considered. Hung et al. [25], Li and Rong [26] investigated the dynamic response of cylindrical shells subjected to UNDEX. And the dynamic responses of plates subjected to UNDEX were also studied by model experiments under terrestrial gravity [27–30]. On the other hand, to physically model an event that is influenced by gravity for the scaled model, the gravity should be scaled in inverse proportion to the prototype [31]. In many cases it may be adequate to test large scale models (e.g., 1/2 or 1/3 scale) under terrestrial gravity [31]. However, for structures such as gravity dams, errors result from improper gravity scaling, which could be significant [31,32]. Further, gravity has a substantial effect on the behavior of bubble oscillation, which means that model tests under the terrestrial gravity condition cannot simultaneously satisfy the similitude requirements of the Mach and Froude numbers [33,34]. Consequently, the centrifuge is a promising tool for UNDEX model tests to meet the similitude requirements.

In the past decades, a few works have been reported in the field of centrifugal UNDEX model tests. Vanadit-Ellis and Davis [35] conducted a series of centrifugal model tests to investigate the failure modes of concrete gravity dams subjected to UNDEX. Hu et al. [34] and Song et al. [36] validated the scaling law for shock wave and bubble oscillation in a centrifuge. Long et al. [37] carried out centrifuge tests and a preliminary numerical study for the dynamic response of a steel plate. On the other hand, the research work on centrifugal UNDEX modeling has not been extensively reported.

To better understand the effect of an UNDEX shock waves on the dynamic responses of an air-backed steel

plate, the present work performed centrifugal model tests and numerical simulation based on ABAQUS to investigate the influence of shock loads. The correlation between the numerical and experimental results were qualitatively and quantitatively investigated. The authors also presented an analysis of the effect of the accumulated shock impulse on the peak strain. The numerical and experimental results suggest that the peak strains are proportional to the accumulated shock impulse.

2 Experimental testing

2.1 Test model

The test model [36] was placed in an alloy container, as shown in Fig. 1. The container was fixed on the centrifuge basket, with an internal size of 1280 mm × 720 mm × 950 mm. The steel plate measured 600 mm × 700 mm × 50 mm and was anchored using cement sand support. The cement support on the right side is a little higher than that on the left side as shown in Fig. 1(b). The container was filled with water 600 mm deep. Dynamic responses were recorded with strain gauges and accelerometers as shown in Fig. 2, where AC-1, AC-2, and AC-3 are the accelerometers.

2.2 Measured shock wave pressure

Fifteen centrifugal UNDEX tests were conducted for different centrifugal accelerations and positions of explosives [34], which are listed in Table 1. W represents the mass of cyclotrimethylenetrinitramine (RDX), which is a powerful explosive; G denotes the centrifugal acceleration, D represents explosion depth, R denotes the distance of the explosive to the pressure sensor, P_m represents the measured peak pressure of shock wave, θ is the measured time delay constant, and L represents the distance of the explosive to the steel plate.

The test of UNDEX-9 was selected for analysis in this work, as the distance from the explosive to the pressure sensor is equal to that from the explosive to the steel plate ($R = L = 250$ mm). Therefore, the measured pressure is considered equivalent to the pressure directly applied on the steel plate, which can be used for calculating the shock response of the steel plate in the numerical model. Figure 3 shows the measured pressure history of UNDEX-9. It can be seen that there are several reflected waves followed by the shock wave because of the wave reflection from the container side walls and the steel plate.

3 Numerical simulation

3.1 UNDEX shock loads

The accuracy of the simulations is strongly dependent on

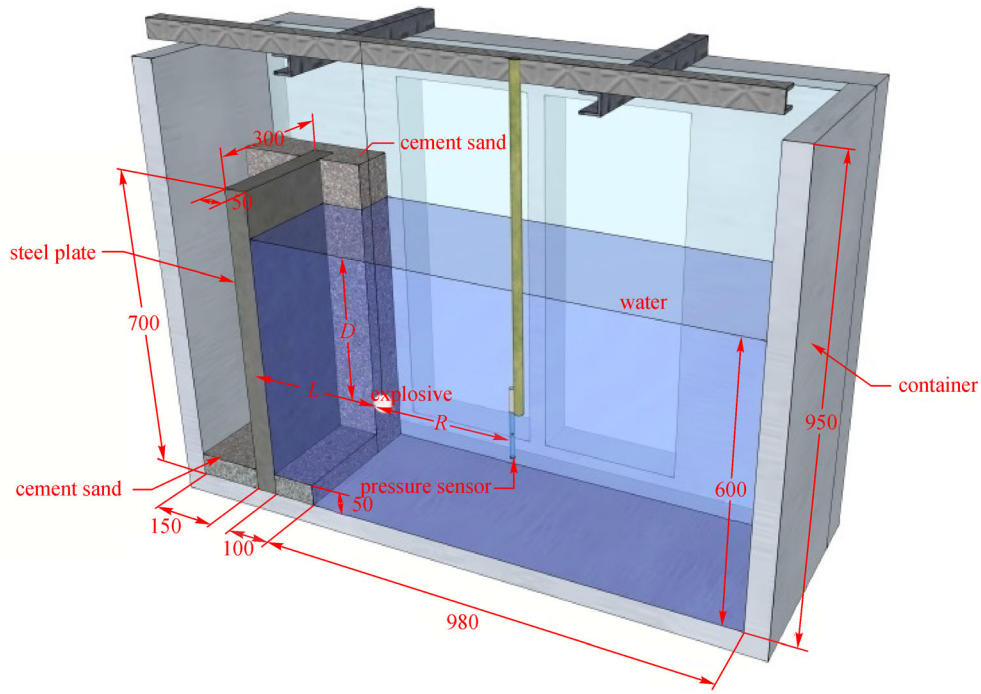


Fig. 1 Test model. (a) 1/2 schematic of model with dimensions (in mm) [36]; (b) actual model.

the shock load history. Cole [2] proposed empirical formulas to describe the history of shock wave pressure as follows.

$$P(t) = P_m e^{-t/\theta}, \tag{1}$$

$$P_m = K_1 \left(\frac{W^{1/3}}{R} \right)^{\alpha_1}, \tag{2}$$

$$\theta = K_2 W^{1/3} \left(\frac{W^{1/3}}{R} \right)^{\alpha_2}, \tag{3}$$

where $P(t)$ denotes the time history of shock wave pressure; P_m represents the peak pressure of shock wave; t is the time; θ is the time delay constant; W is the mass of explosive; R is the distance of the explosive to the measured point (pressure sensor); K_1 , K_2 , α_1 , and α_2 are coefficients to be determined experimentally. The detail values of the P_m , W , θ , and R for test cases are listed in Table 1.

The values of K_1 , K_2 , α_1 , and α_2 can be fitted from the experimental results, which are 73.760, 42.838, 1.143, and -0.738 , respectively, as shown in Fig. 4.

To improve Cole’s formulas, Zamyshlyaev and Yakovlev [38] proposed the formulas to predict the time history

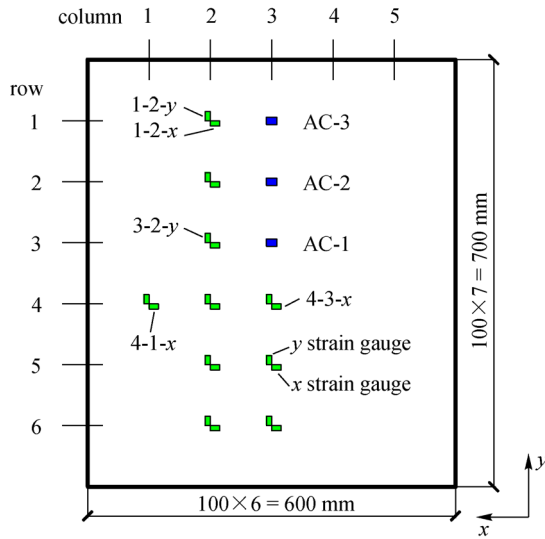


Fig. 2 Layout of transducers on the downstream surface.

of the shock wave pressure [5,38–40]. Figure 5 shows the pressure time histories of Zamyshlyayev and Yakovlev’s form and Cole’s form compared with the measured.

The relative difference (D_r) of the peak pressure of Zamyshlyayev and Yakovlev’s load is larger than that of Cole’s load, as listed in Table 2.

According to Fig. 5, the attenuating speed of the peak shock pressure corresponding to Zamyshlyayev and Yakovlev’s form is lower than that of Cole’s form, which is closer to the measured pressure at the tail stage. Therefore, the characterization of the influences of the shock load history or peak pressure of the shock load on the accuracy of the numerical results deserves careful study.

3.2 Description of numerical model

With the help of ABAQUS, the “scattered wave” formula [17,40] was used to study the dynamic response of the steel plate. Water is modeled as a kind of acoustic medium, which leads to less computing time since the pressure, instead of the displacement, is considered as the degree of freedom for the fluid acoustic element [40]. The pressure time history at the contact point between fluid and structure where the shock wave reaches first must be calculated first; then, the pressure field in other zones of the fluid will be worked out. Finally, the pressure field in the fluid is applied directly to the structure surface [41,42]. Therefore, the fluid field that is far from the structure has little effect on the dynamic response of the steel plate, and the extent of the water domain can be truncated as shown in Fig. 6 to reduce the computational intensity. The steel plate and the cement sand are simulated by the C3D8R eight-node solid element, and the fluid is simulated by the AC3D8R acoustic element.

According to the experimental setups, the boundaries of the cement sand are considered fixed. Surface-to-surface contact was applied between the cement sand and the steel plate. The “TIE” constraint was applied to the interface of the water and the steel plate. The initial pressure of the free surface of water is defined as zero, and the water boundary surfaces were set to be non-reflecting as the reflected waves have been considered in the incident wave history itself. The shock loads associated with the numerical model are described in Figs. 3 and 5. The relevant material parameters adopted in the numerical model are listed in Table 3.

To validate the accuracy of the numerical analysis, three

Table 1 Test cases

group	UNDEX-	W (g)	G (g)	D (m)	R (mm)	P_m (MPa)	θ (μ s)	L (mm)
I	3	1.025	40	0.30	350	17.62	8.175	300
	4	1.023	40	0.30	350	18.17	7.437	300
	6	1.015	40	0.30	300	21.48	9.621	200
	9	1.024	40	0.30	250	25.45	9.206	250
	10	1.010	40	0.30	175	36.99	7.684	150
	11	1.025	40	0.30	150	49.32	7.344	50
II	1	1.020	20	0.30	350	19.44	9.514	300
	2	1.021	30	0.30	350	18.31	10.077	300
	5	1.038	50	0.30	350	19.34	10.233	300
	7	1.040	40	0.20	300	21.29	9.900	200
	8	1.016	20	0.20	300	20.19	9.229	200
	15	0.050	20	0.30	350	3.47	8.953	300
	13	0.050	30	0.25	353.6	3.07	9.192	300
	12	0.150	20	0.375	357.9	5.83	10.639	300
	14	0.150	40	0.30	350	4.99	10.429	300

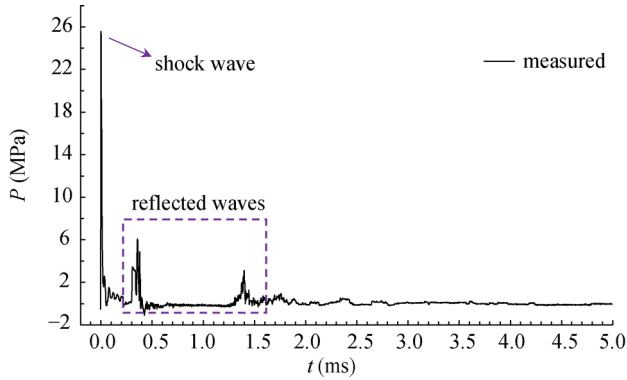


Fig. 3 History of the measured shock wave pressure of UNDEX-9.

models with the element size of 1.0, 0.8, and 0.5 cm for the steel plate were developed. The strain time histories of the numerical results are shown in Fig. 7. It shows that the strain time history of the steel plate with the element size of 1.0 cm is close to those with the element size of 0.8 and 0.5 cm.

Based on a combination of accuracy and computational intensity, 1.0 cm mesh was selected for the steel plate used in the numerical model. The element size of cement sand

and water is 1.0 and 0.5 cm, respectively. There are 425934 nodes and 394490 elements in the whole model.

3.3 Results and discussion

3.3.1 Strain

Due to the symmetry of the model, the strain time histories at the points on one half of the steel plate were recorded. Figure 8 is the strain contour of the steel plate, which shows the propagation of the stress wave in the steel plate.

The comparison of the strain time histories of the numerical and experimental results is shown in Fig. 9. It is clearly shown that the numerical results obtained from Zamyshlyayev and Yakovlev’s load and the measured load agree better with the test results than those obtained from the Cole’s load. However, the simulated strain time histories differ greatly with the experimental results from 2 to 6 ms. This may have been caused by the improper time history of the reflected wave since there was no reflected wave for Cole’s load and Zamyshlyayev and Yakovlev’s load. Moreover, the reflected waves of the measured load by the pressure sensor cannot reveal the reflected waves applied on the steel plate correctly. On the other hand, the

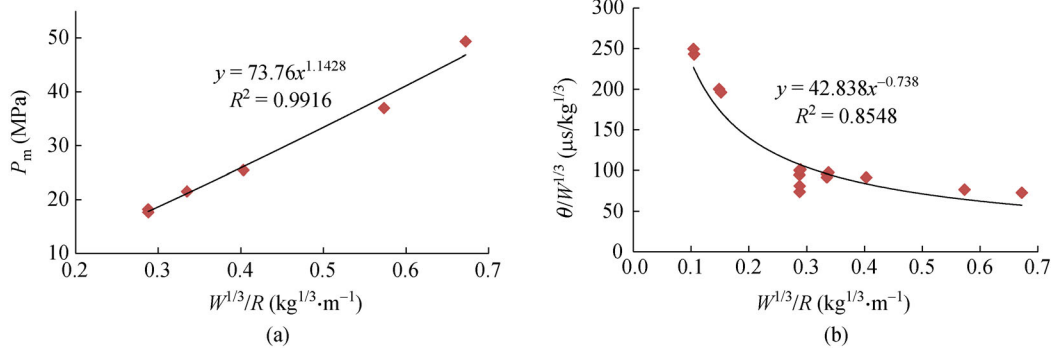


Fig. 4 Relationship between (a) peak pressure (data come from Group I) and (b) time delay constant with scaled distance.

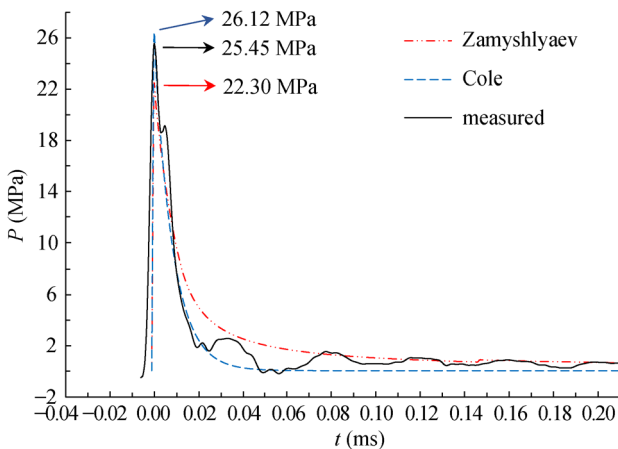


Fig. 5 Histories of the shock loads.

Table 2 Peak pressure

item	measured	Cole	Zamyshlyayev
peak pressure (MPa)	25.45	26.12	22.30
relative difference D_r	–	2.6%	12.4%

Table 3 Material parameters

material	density (kg/m ³)	Young’s/bulk modulus (GPa)	Poisson’s ratio
steel plate	8714	206	0.3
cement sand	2400	29.5	0.3
water	1000	2.14	–

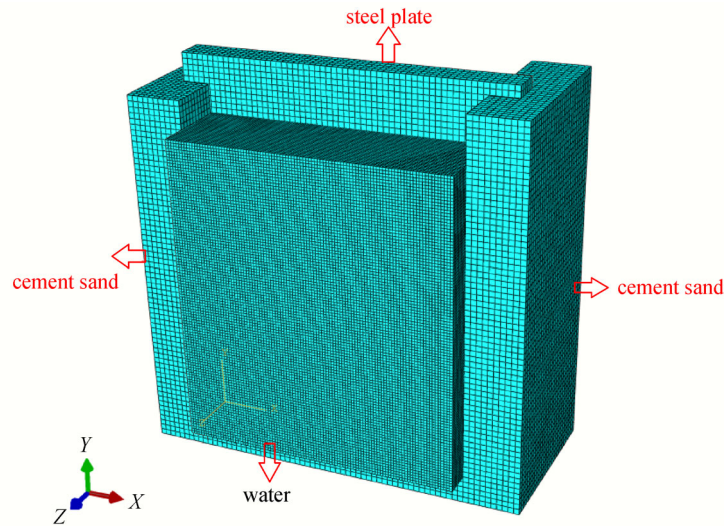


Fig. 6 Numerical model of the experiments.

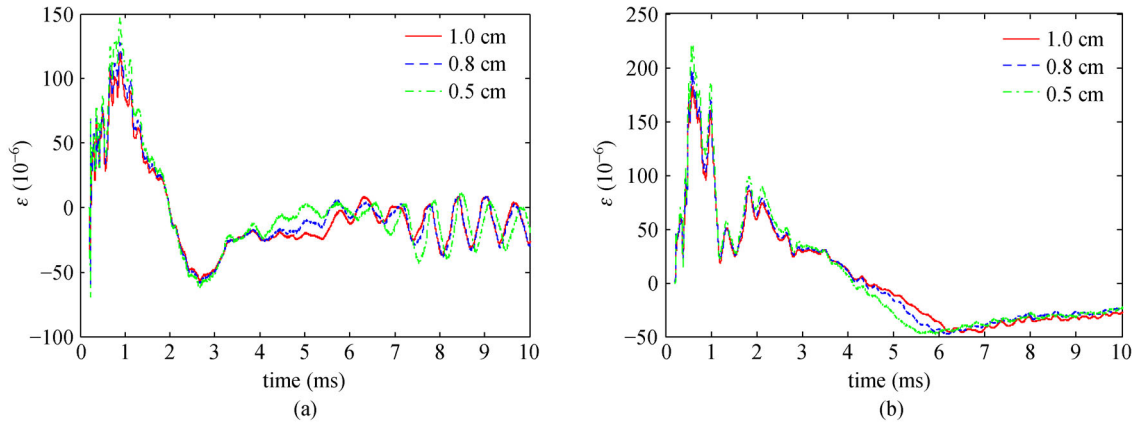


Fig. 7 Strain time histories of the steel plate with different element sizes. (a) 4-2-x and (b) 4-2-y.

boundary condition may also lead to the greater error of numerical results from 2 to 6 ms. Because the steel plate was imbedded in the cement supports, the real boundary is complicated. This can cause problems that cannot be effectively reflected in the numerical simulation by fixed or simply supported boundary conditions.

The peak strains obtained from numerical simulations are listed in Table 4. Notably, the average relative percentage differences D_r of the simulated peak strains obtained from the measured load, Cole’s load, and Zamyshlyayev and Yakovlev’s load are 21.39%, 45.73%, and 13.92%, respectively.

The Russell error technique [43], a method to evaluate the differences between two transient data sets by quantifying the variation in magnitude and phase, was used to make quantitative assessments for the three numerical results. The magnitude error and the phase

error were then combined into a single error measurement, i.e., the comprehensive error factor. The phase error RP , magnitude error RM , and the comprehensive error RC are given as follows:

$$RP = \frac{1}{\pi} \cos^{-1} \left(\frac{\sum c_i m_i}{\sqrt{\sum c_i^2 \sum m_i^2}} \right), \quad (4)$$

$$RM = \text{sign}(m) \log_{10}(1 + |m|), \quad (5)$$

$$RC = \sqrt{\frac{\pi}{4}(RM^2 + RP^2)}, \quad (6)$$

where c_i and m_i represent the numerical results and the test results, respectively, and m is defined by

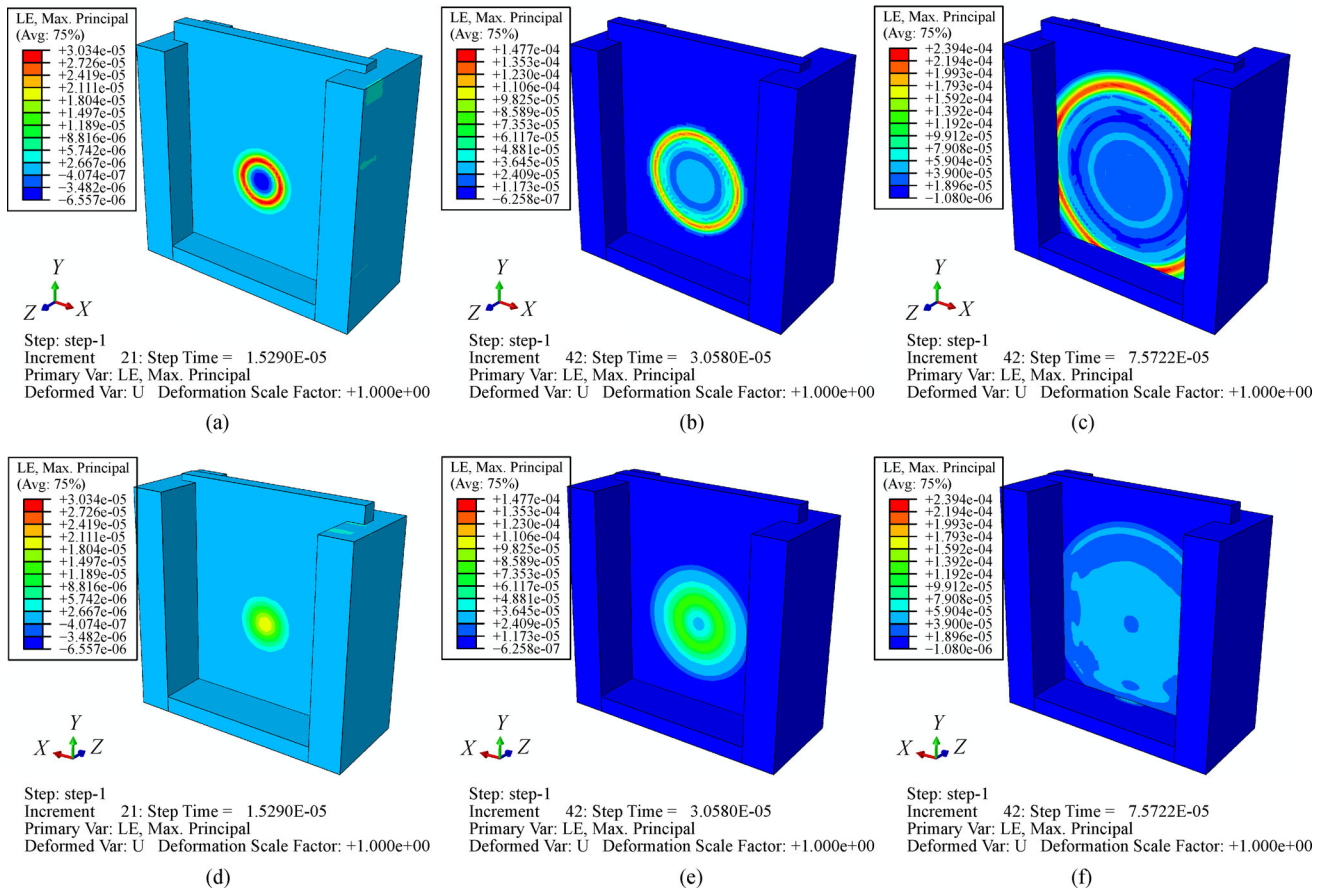


Fig. 8 The strain contour of the steel plate on the upstream surface. (a) $t = 0.015$ ms; (b) $t = 0.030$ ms; (c) $t = 0.076$ ms. For the downstream surface: (d) $t = 0.015$ ms; (e) $t = 0.030$ ms; (f) $t = 0.076$ ms.

Table 4 Peak strains of the experimental and numerical results

item	test (10^{-6})	numerical: measured (10^{-6})	D_{r-M} (%)	numerical: Cole (10^{-6})	D_{r-C} (%)	numerical: Zamyshlyayev (10^{-6})	D_{r-Z} (%)
3-2-x	137.57	171.57	24.71	54.30	60.53	141.39	2.78
3-2-y	155.68	218.92	40.62	103.87	33.28	186.97	20.10
4-2-x	123.56	147.29	19.21	72.92	40.98	119.11	3.60
4-2-y	216.17	207.82	3.86	108.91	49.62	184.03	14.87
4-3-x	170.14	270.20	58.81	78.07	54.11	218.71	28.55
4-3-y	187.47	242.19	29.19	139.05	25.83	226.56	20.85
5-2-x	115.92	106.14	8.43	52.96	54.31	90.75	21.71
5-2-y	170.50	186.79	9.56	100.66	40.96	171.26	0.45
5-3-x	190.93	203.21	6.43	63.60	66.69	163.84	14.19
5-3-y	184.48	208.55	13.05	127.23	31.03	206.76	12.08

$$m = \frac{\sum c_i^2 - \sum m_i^2}{\sqrt{\sum c_i^2 \sum m_i^2}} \quad (7)$$

Excellent, good, acceptable, and poor correlations between the numerical results and the test results are defined as $RC \leq 0.15$, $0.15 < RC \leq 0.2$, $0.2 < RC \leq 0.28$, and $RC > 0.28$, respectively [14,44]. The comprehensive errors of the three numerical results are listed in Table 5.

Table 5 Comprehensive errors RC of the strains of three numerical results

item	measured	assessment	Cole	assessment	Zamyshlyayev	assessment
3-2-x	0.207	acceptable	0.645	poor	0.222	acceptable
3-2-y	0.287	poor	0.473	poor	0.210	acceptable
4-2-x	0.189	good	0.657	poor	0.218	acceptable
4-2-y	0.267	acceptable	0.538	poor	0.211	acceptable
4-3-x	0.210	acceptable	0.634	poor	0.217	acceptable
4-3-y	0.260	acceptable	0.504	poor	0.173	good
5-2-x	0.335	poor	0.757	poor	0.354	poor
5-2-y	0.245	acceptable	0.534	poor	0.197	good
5-3-x	0.297	poor	0.718	poor	0.319	poor
5-3-y	0.239	acceptable	0.540	poor	0.216	acceptable

Table 5 suggests the simulated strain time histories obtained from Cole’s load have poor correlation with the test results, while the simulated strain time histories obtained from the measured load and Zamyshlyayev and Yakovlev’s load have acceptable agreement with the test results. In conclusion, it can be considered that among the three loads, the numerical results obtained from Zamyshlyayev and Yakovlev’s load had the best correlation, followed by those obtained from the measured load. Moreover, the numerical results obtained from Cole’s load had the worst correlation with the test results, even though the peak pressure of Cole’s load showed a smaller relative difference. Therefore, the overall trend of the load history plays a dominant role in the simulated strains instead of the peak pressure.

3.3.2 Effect of accumulated shock impulse on peak strain

Generally, each shock wave and bubble oscillation accounts for nearly 50% of the explosive energy [10,34], and both of them can cause structural damage. The result in Ref. [37] shows that, the peak pressure induced by the shock wave for 1 g RDX is nearly 20 times larger than that induced by the bubble oscillation, while the peak strain of the steel plate induced by the shock wave is approximately equivalent to that induced by the bubble oscillation. Obviously, the essential contributor to the accuracy of the simulated strains is not the peak pressure of the shock wave but the shock impulse. The corresponding formulas of the shock impulse I per unit area and the accumulated shock impulse I_a per unit area are defined as follows.

$$I(t) = \int_0^t P(t)dt, \tag{8}$$

$$I_a = \int_0^t I(t)dt. \tag{9}$$

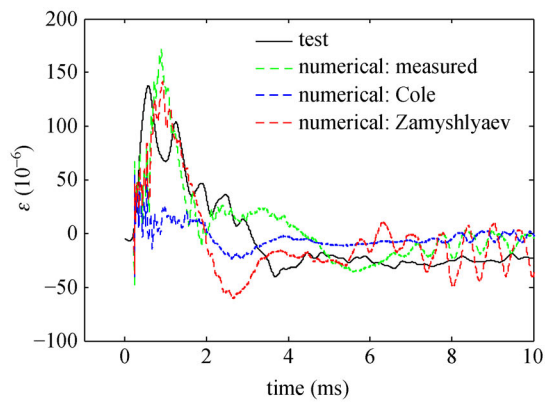
Figure 10 shows the shock impulse I and the

accumulated shock impulse I_a of the three shock loads. It can be found from Fig. 10(b) that the respective values of I_a in descending order are obtained from the measured load, Zamyshlyayev and Yakovlev’s load, and Cole’s load at approximately 0.8 ms. A similar trend was also detected for the peak strains listed in Table 4. Thus, it can be summarized that the peak strains may be proportional to I_a when the time $t = t_{ps}$. Herein t_{ps} is the time when the strain of the plate for every point reaches the peak value.

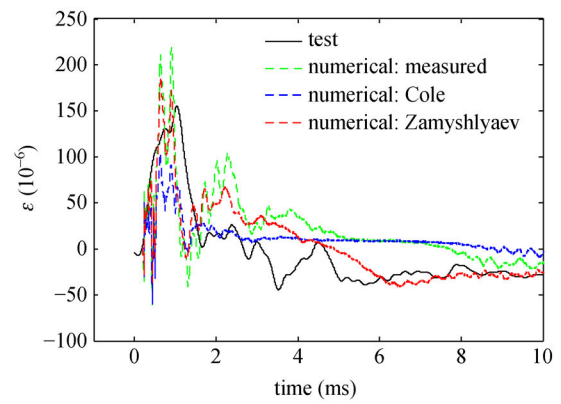
According to Cole’s calculations and Zamyshlyayev and Yakovlev’s formulas, the shock impulse and the accumulated shock impulse depend on the scale distance $Z = L/W^{1/3}$, where W is the explosive mass and L is the distance from the explosive to the steel plate. To validate this conclusion, seven UNDEX shock loads calculated from Zamyshlyayev and Yakovlev’s formulas were applied to the numerical model to obtain the respective peak strains, as shown in Fig. 11. The average values of comprehensive error RC of 4-2-x, 4-2-y, 4-3-x, and 4-3-y are smaller than those of others as shown in Table 5, which show a good correlation of the numerical results with the experimental results. Thus, the peak strains S_m of points 4-2-x, 4-2-y, 4-3-x, and 4-3-y were chosen for analysis.

When the strains of the steel plate reached their peak values, the peak strains S_m and the corresponding accumulated shock impulse I_a were calculated and are listed in Table 6.

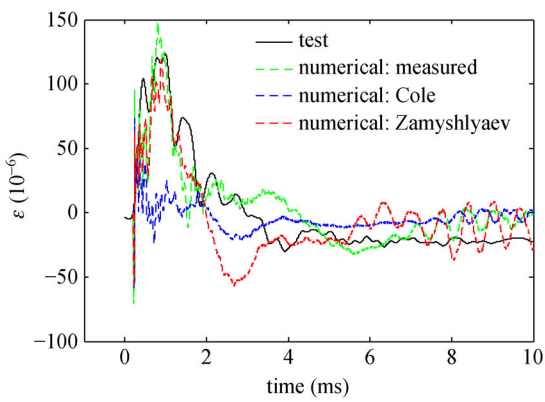
The relationships between the peak strains and the accumulated shock impulses obtained from numerical simulation are depicted in Fig. 12, which shows good agreement between the experimental and the numerical results, except for the strains of 4-2-y and 4-3-y of UNDEX-10. The peak strain is apparently proportional to the accumulated shock impulse. The fitted relationships between the peak strains S_m and the accumulated shock impulse I_a of 4-2-x, 4-2-y, 4-3-x, and 4-3-y are $S_m = 714.0I_a - 92.2$, $S_m = 1089.2I_a - 1.7$, $S_m = 1237.9I_a - 36.0$, and $S_m = 1480.6I_a - 27.1$, respectively. Therefore, the



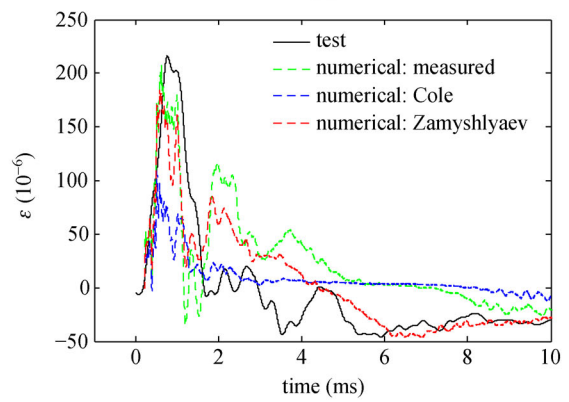
(a)



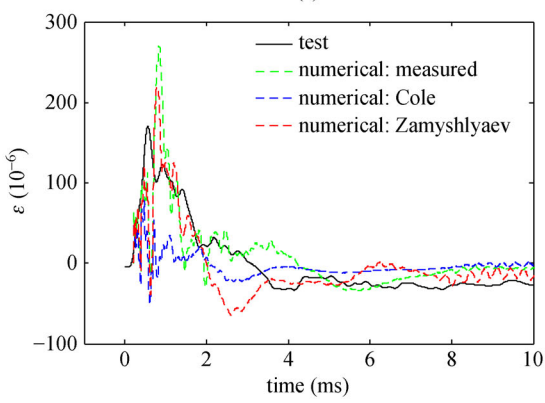
(b)



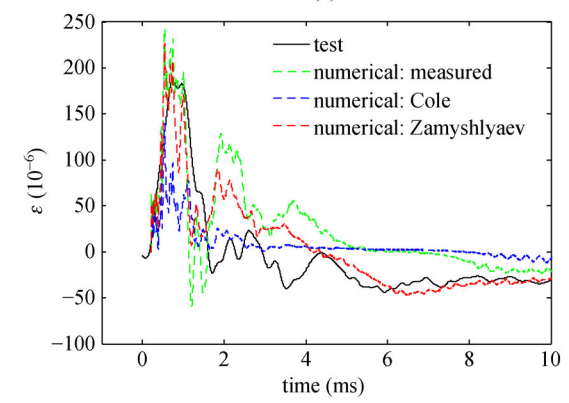
(c)



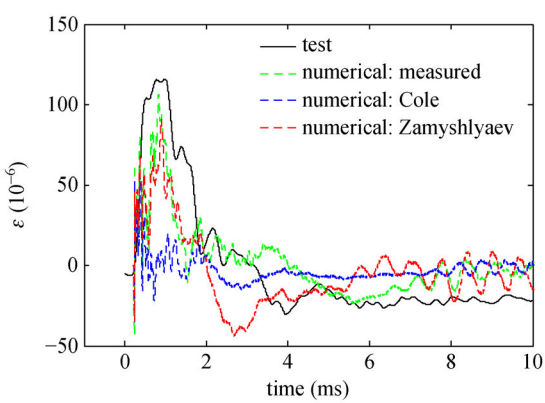
(d)



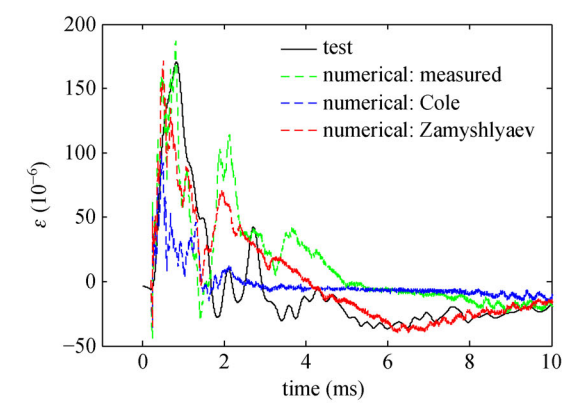
(e)



(f)



(g)



(h)

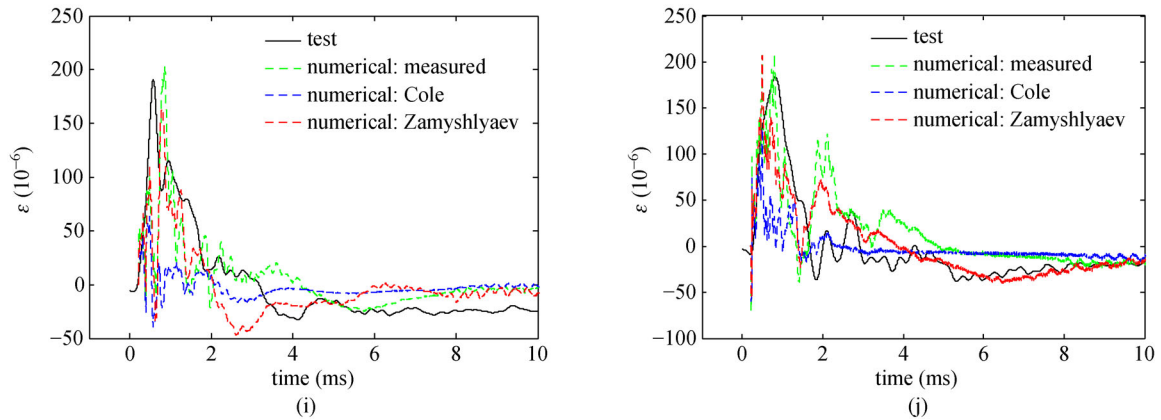


Fig. 9 The time histories of the strain. (a) 3-2-x; (b) 3-2-y; (c) 4-2-x; (d) 4-2-y; (e) 4-3-x; (f) 4-3-y; (g) 5-2-x; (h) 5-2-y; (i) 5-3-x; (j) 5-3-y.

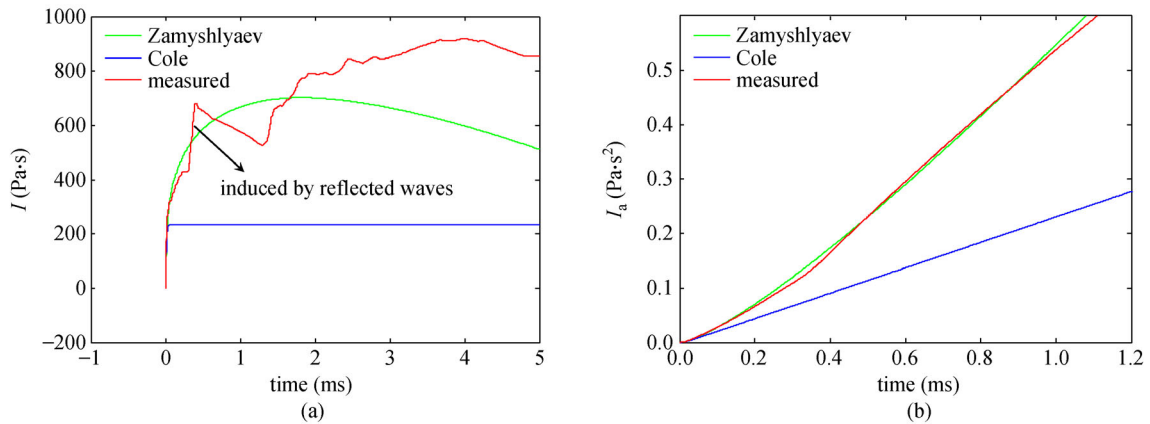


Fig. 10 The time histories of the (a) pressure impulse and (b) the accumulated shock impulse.

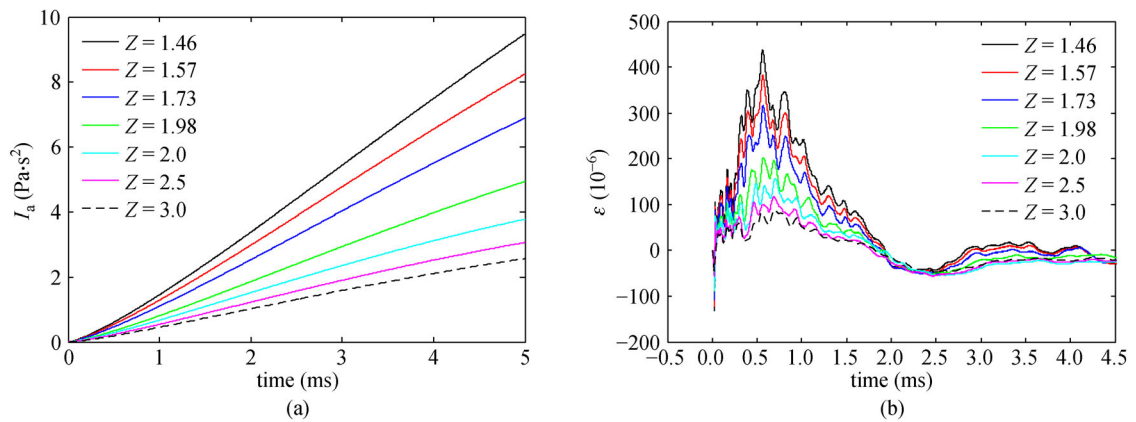


Fig. 11 The time histories of the (a) accumulated shock impulse and (b) the corresponding strain 4-2-x.

assumption mentioned above has been well validated. It should be noted that the relationship may not be suitable for a much smaller scaled distance Z due to the limitation of Zamyshlyayev and Yakovlev's formulas.

4 Conclusions

In this work, the numerical simulation and centrifugal model tests were performed to investigate the effects of

Table 6 Peak strains S_m and corresponding accumulated shock impulse I_a

item	Z (m/kg ^{1/3})	L (m)	W (g)	4-2-x		4-2-y		4-3-x		4-3-y	
				I_a (Pa·s ²)	S_m (10 ⁻⁶)						
numerical	1.46	0.25	5.000	0.70	438.51	0.43	493.24	0.63	792.67	0.39	635.39
	1.57	0.25	4.000	0.63	381.92	0.38	439.33	0.56	714.43	0.35	563.93
	1.73	0.25	3.000	0.54	316.36	0.33	377.74	0.48	615.84	0.30	481.39
	1.98	0.25	2.000	0.40	202.70	0.24	270.85	0.36	410.22	0.22	342.83
	2.00	0.20	1.000	0.44	157.44	0.22	216.29	0.33	267.71	0.19	287.21
	2.50	0.25	1.000	0.34	117.00	0.16	181.54	0.28	213.35	0.14	224.06
	3.00	0.30	1.000	0.29	88.33	0.13	150.53	0.26	158.96	0.12	188.19
UNDEX-10	1.50	0.15	1.010	0.52	269.37	0.47	348.02	0.32	279.81	0.47	308.83
UNDEX-6	1.99	0.20	1.015	0.34	202.00	0.31	310.63	0.18	239.11	0.30	267.78
UNDEX-9	2.48	0.25	1.024	0.42	123.56	0.28	216.17	0.16	170.14	0.28	187.47
UNDEX-3	2.98	0.30	1.025	0.27	103.75	0.17	207.44	0.08	156.47	0.16	174.66
UNDEX-4	2.98	0.30	1.023	0.22	140.25	0.17	204.27	0.09	155.04	–	–

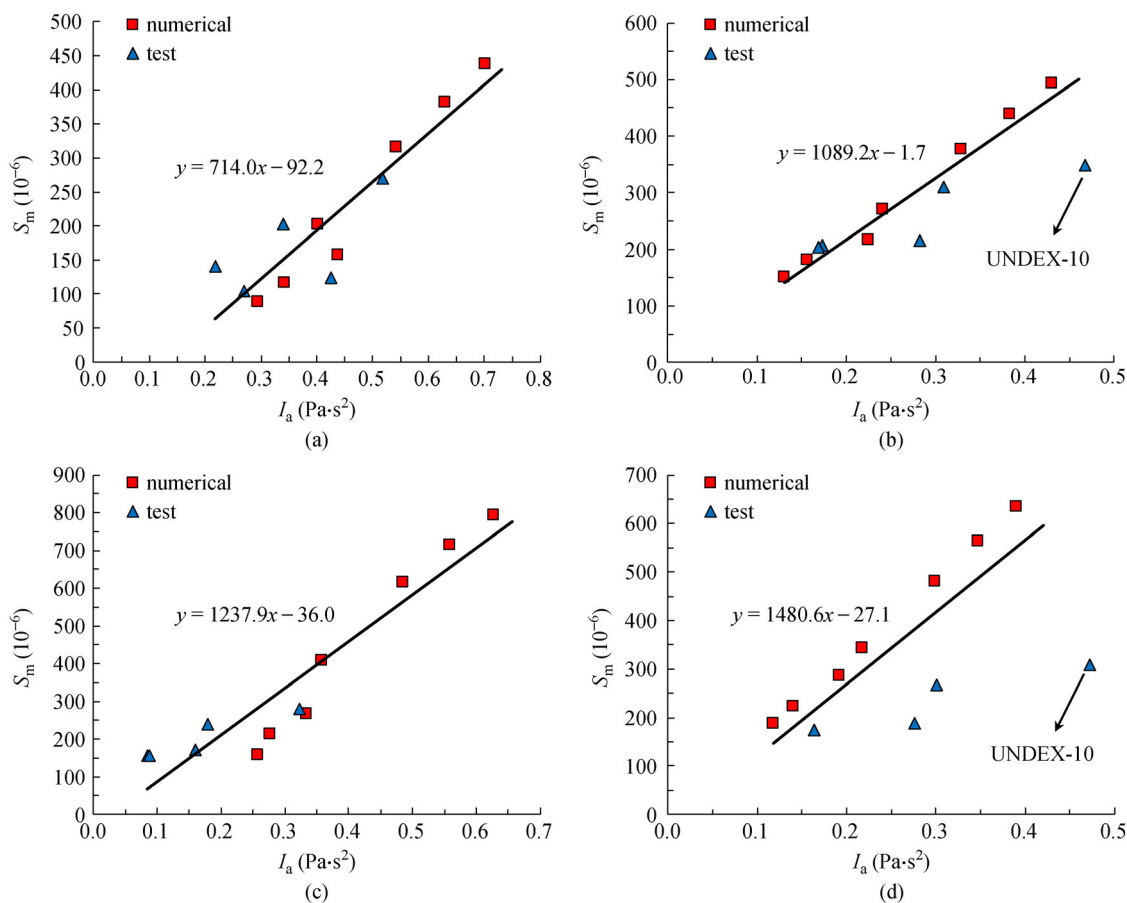


Fig. 12 The relationship between the peak strains S_m and the accumulated shock impulse I_a . (a) 4-2-x; (b) 4-2-y; (c) 4-3-x; (d) 4-3-y.

UNDEX shock loads on the dynamic response of an air-backed steel plate. The simulated strain time histories of the steel plate obtained from the measured load, Cole’s load and Zamyshlyaev and Yakovlev’s load are compared

to the test values. The Russell error technique was used to quantitatively analyze the correlation between the strain time histories of numerical and experimental results. In addition, the effect of the accumulated shock pressure

impulse on the peak strains was also investigated. Based on the experimental and numerical analysis, the following conclusions are drawn.

1) The four coefficients K_1 , K_2 , α_1 , and α_2 of Cole's formulas for the RDX explosive are determined by testing, the values of which are 73.760, 42.838, 1.143, and -0.738 .

2) The simulated strain time histories obtained from the measured load and Zamyshlyayev and Yakovlev's load are consistent with the test results, while those obtained from Cole's load are not. The average relative percentage differences (D_r) of the simulated peak strains obtained from the measured load, Cole's load, and Zamyshlyayev and Yakovlev's load are 21.39%, 45.73%, and 13.92%, respectively.

3) Based on the comprehensive errors of the numerical results, the simulated strain time histories obtained from Zamyshlyayev and Yakovlev's load have the best correlation with the test, followed by those obtained from the measured load, and the lowest are those obtained from Cole's load. The trend of the load history plays a dominant role in the simulated strains instead of the peak pressure.

4) The numerical peak strain S_m was proportional to the accumulated shock impulse I_a when the strain reached the peak value, and the relationships corresponding to points 4-2-x, 4-2-y, 4-3-x, and 4-3-y were $S_m = 714.0I_a - 92.2$, $S_m = 1089.2I_a - 1.7$, $S_m = 1237.9I_a - 36.0$, and $S_m = 1480.6I_a - 27.1$, respectively.

Acknowledgements This work was supported by the State Key Program of the National Natural Science Foundation of China (Grant No. 51339006).

References

- Kirkwood J G, Bethe H A. Basic Propagation Theory. OSRD, 1942, 588–595
- Cole R H. Underwater Explosions. New Jersey: Princeton University Press, 1948
- Keil A H. The Response of Ships to Underwater Explosions. Washington D.C.: David Taylor Model Basin, 1961
- Reid W D. The Response of Surface Ships to Underwater Explosions. Defence Science and Technology Organization Canberra, 1996
- Jin Q K, Ding G Y. A finite element analysis of ship sections subjected to underwater explosion. *International Journal of Impact Engineering*, 2011, 38(7): 558–566
- Rabczuk T, Gracie R, Song J H, Belytschko T. Immersed particle method for fluid-structure interaction. *International Journal for Numerical Methods in Engineering*, 2010, 81(1): 48–71
- Vu-Bac N, Lahmer T, Zhuang X Y, Nguyen-Thoi T, Rabczuk T. A software framework for probabilistic sensitivity analysis for computationally expensive models. *Advances in Engineering Software*, 2016, 100: 19–31
- Kwon Y W, Cunningham R E. Comparison of USA-DYNA finite element models for a stiffened shell subject to underwater shock. *Computers & Structures*, 1998, 66(1): 127–144
- Gong S W, Lam K Y. Transient response of floating composite ship section subjected to underwater shock. *Composite Structures*, 1999, 46(1): 65–71
- Zhang A M, Zhou W X, Wang S P, Feng L H. Dynamic response of the non-contact underwater explosions on naval equipment. *Marine Structures*, 2011, 24(4): 396–411
- Schiffer A, Tagarielli V L. The dynamic response of composite plates to underwater blast: Theoretical and numerical modelling. *International Journal of Impact Engineering*, 2014, 70: 1–13
- Shin Y S. Ship shock modeling and simulation for far-field underwater explosion. *Computers & Structures*, 2004, 82(23–26): 2211–2219
- LeBlanc J, Shukla A. Dynamic response and damage evolution in composite materials subjected to underwater explosive loading: An experimental and computational study. *Composite Structures*, 2010, 92(10): 2421–2430
- LeBlanc J, Shukla A. Dynamic response of curved composite panels to underwater explosive loading: Experimental and computational comparisons. *Composite Structures*, 2011, 93(11): 3072–3081
- Kwon Y W, Fox P K. Underwater shock response of a cylinder subjected to a side-on explosion. *Computers & Structures*, 1993, 48(4): 637–646
- Cichocki K. Effects of underwater blast loading on structures with protective elements. *International Journal of Impact Engineering*, 1999, 22(6): 609–617
- Zong Z, Zhao Y, Li H T. A numerical study of whole ship structural damage resulting from close-in underwater explosion shock. *Marine Structures*, 2013, 31: 24–43
- Arora H, Del Linz P, Dear J P. Damage and deformation in composite sandwich panels exposed to multiple and single explosive blasts. *International Journal of Impact Engineering*, 2017, 104: 95–106
- Rabczuk T, Belytschko T. A three-dimensional large deformation meshfree method for arbitrary evolving cracks. *Computer Methods in Applied Mechanics and Engineering*, 2007, 196(29–30): 2777–2799
- Rabczuk T, Areias P M A, Belytschko T. A meshfree thin shell method for non-linear dynamic fracture. *International Journal for Numerical Methods in Engineering*, 2007, 72(5): 524–548
- Rabczuk T, Zi G, Bordas S, Nguyen-Xuan H. A simple and robust three-dimensional cracking-particle method without enrichment. *Computer Methods in Applied Mechanics and Engineering*, 2010, 199(37–40): 2437–2455
- Hamdia K M, Silani M, Zhuang X Y, He P F, Rabczuk T. Stochastic analysis of the fracture toughness of polymeric nanoparticle composites using polynomial chaos expansions. *International Journal of Fracture*, 2017, 206(2): 215–227
- Hamdia K M, Ghasemi H, Zhuang X Y, Alajlan N, Rabczuk T. Sensitivity and uncertainty analysis for flexoelectric nanostructures. *Computer Methods in Applied Mechanics and Engineering*, 2018, 337: 95–109
- De A, Zimmie T F. Centrifuge modeling of surface blast effects on underground structures. *Geotechnical Testing Journal*, 2007, 30(5): 427–431
- Hung C F, Lin B J, Hwang-Fuu J J, Hsu P Y. Dynamic response of cylindrical shell structures subjected to underwater explosion.

- Ocean Engineering, 2009, 36(8): 564–577
26. Li J, Rong J L. Experimental and numerical investigation of the dynamic response of structures subjected to underwater explosion. *European Journal of Mechanics-B/Fluids*, 2012, 32: 59–69
 27. Ramajeyathilagam K, Vendhan C P, Rao V B. Non-linear transient dynamic response of rectangular plates under shock loading. *International Journal of Impact Engineering*, 2000, 24(10): 999–1015
 28. Ramajeyathilagam K, Vendhan C P. Deformation and rupture of thin rectangular plates subjected to underwater shock. *International Journal of Impact Engineering*, 2004, 30(6): 699–719
 29. Rajendran R, Narasimhan K. Linear elastic shock response of plane plates subjected to underwater explosion. *International Journal of Impact Engineering*, 2001, 25(5): 493–506
 30. Hung C F, Hsu P Y, Hwang-Fuu J J. Elastic shock response of an air-backed plate to underwater explosion. *International Journal of Impact Engineering*, 2005, 31(2): 151–168
 31. Kutter B L, O’Leary L M, Thompson P Y, Lather R. Gravity-scaled tests on blast-induced soil-structure interaction. *Journal of Geotechnical Engineering*, 1988, 114(4): 431–447
 32. Plizzari G, Waggoner F, Saouma V E. Centrifuge modeling and analysis of concrete gravity dams. *Journal of Structural Engineering*, 1995, 121(10): 1471–1479
 33. Snay H G. The scaling of underwater explosion phenomena. White Oak, MD: Naval Ordnance Lab, 1962
 34. Hu J, Chen Z Y, Zhang X D, Wei Y Q, Liang X Q, Liang J H, Ma G W, Wang Q S, Long Y. Underwater explosion in centrifuge part I: Validation and calibration of scaling laws. *Science China. Technological Sciences*, 2017, 60(11): 1638–1657
 35. Vanadit-Ellis W, Davis L K. Physical modeling of concrete gravity dam vulnerability to explosions. In: *Waterside Security Conference (WSS)*. Carrara, 2010: 1–11
 36. Song G, Chen Z Y, Long Y, Zhong M S, Wu J Y. Experimental and numerical investigation of the centrifugal model for underwater explosion shock wave and bubble pulsation. *Ocean Engineering*, 2017, 142: 523–531
 37. Long Y, Zhou H Y, Liang X Q, Song G, Chen Z Y, Hu J, Wang Q S, Zhang X D, Liang J H, Huang Z J. Underwater explosion in centrifuge Part II: Dynamic responses of defensive steel plate. *Science China. Technological Sciences*, 2017, 60(12): 1941–1957
 38. Zamyshlyayev B V, Yakovlev Y S. *Dynamic Loads in Underwater Explosion*. Naval Intelligence Support Center Washington D. C. Translation Div, 1973
 39. Zhang Z H, Wang Y, Zhang L J, Yuan J H, Zhao H F. Similarity research of anomalous dynamic response of ship girder subjected to near field underwater explosion. *Applied Mathematics and Mechanics*, 2011, 32(12): 1491–1504
 40. Zong Z, Zhao Y J, Zou L. *Numerical Computation for Structural Damages of Underwater Explosion*. Beijing: Science Press, 2014 (in Chinese)
 41. Yao X L, Zhang A M, Xu W J. Application of coupled acoustic-structural analysis to warship underwater explosion. *Journal of Harbin Engineering University*, 2005, 26(6): 707–712 (in Chinese)
 42. Xu Y G, Zong Z, Li H T. Numerical analysis of structure response due to the combined effects of underwater explosion shock wave and bubble pulse. *Chinese Journal of Ship Research*, 2011, 6(3): 8–11 (in Chinese)
 43. Russell D M. Error measures for comparing transient data: Part I: development of a comprehensive error measure. In: *Proceedings of the 68th Shock and Vibration Symposium*. Hunt Valley, MD, 1997, 175–184
 44. Lee A S, Kim B O, Kim Y C. A finite element transient response analysis method of a rotor-bearing system to base shock excitations using the state-space Newmark scheme and comparisons with experiments. *Journal of Sound and Vibration*, 2006, 297(3–5): 595–615